Extreme Mechanics Letters 32 (2019) 100544

Contents lists available at ScienceDirect

Extreme Mechanics Letters

journal homepage: www.elsevier.com/locate/eml

Control of underwater acoustics using anisotropic solid metamaterials with continuously tuned material axes

Yong Cheng, Tianjun Yu, Xiaoming Zhou *

Key Laboratory of Dynamics and Control of Flight Vehicle, Ministry of Education and School of Aerospace Engineering, Beijing Institute of Technology, Beijing 100081, China

ARTICLE INFO

Article history:
Received 30 May 2019
Received in revised form 16 August 2019
Accepted 16 August 2019
Available online 19 August 2019

Keywords:
Transformation acoustics
Acoustic metamaterials
Anisotropic density

ABSTRACT

Inertial transformation acoustics is a method for deriving a spatial pattern of material parameters for use in the arbitrary regulation of acoustic trajectories. This work highlights the discussion on a general metamaterial model with material properties that meet all the needs of the inertial transformation parameters. The proposed solid metamaterials are described to possess broadband anisotropic density and continuously tuned material axis while exhibiting fluid-like elasticity, namely, isotropic bulk stiffness and sufficiently small shear resistance. In particular, the metamaterial structure embodies a regular cell shape with an unaltered profile against the rotation of material axes, which facilitates the assembly of functional devices. An underwater acoustic rotator is designed and numerically verified to elucidate the wave dispersion and effective-medium characteristics of the metamaterial. A guideline for constructing the transformation device from the basic cells is also provided herein. The presented model can serve as a new material platform on the exploration of arbitrary acoustic-control via the inertial transformation method.

1. Introduction

Transformation acoustics has shown great potential in manipulating acoustic propagation, which not only inspired novel wave functionalities (*e.g.,* acoustic cloaking) [1–5] but also advanced the development of new material and structure design [6–8]. The transformation method was established on the basis of the form invariance of classical wave equations under a coordinate mapping. Maxwell's equation, which governs electromagnetic wave propagation, was found to maintain rigorously the same form [9]. On the contrary, transformation acoustic materials are not uniquely defined and, as such, there exist more flexibilities to design sound devices. Recall that for a spatial mapping from $\boldsymbol{X}$ to $\boldsymbol{x}'$, acoustic Helmholtz equation, *i.e.,* $\kappa_0\nabla^2 p-\rho_0\ddot{p}=0$, is transformed into the general pentamode-inertial expression, [10]

$$\kappa\boldsymbol{S}:\nabla\left[\boldsymbol{\rho}^{-1}\nabla\cdot(\boldsymbol{S}p)\right]-\ddot{p}=0, \tag{1}$$

where the pseudo-pressure p is related to the strain $\boldsymbol{\varepsilon}$ by $p=-\kappa\,\mathrm{tr}\,(\boldsymbol{S}\boldsymbol{\varepsilon})$ with $\kappa=\kappa_0 J$. Accordingly, the mass density $\boldsymbol{\rho}$ and stiffness $\boldsymbol{C}$ are given by,

$$\boldsymbol{\rho}^{-1}=\rho_0^{-1}J^{-1}\boldsymbol{S}^{-1}\boldsymbol{F}\boldsymbol{F}^T\boldsymbol{S}^{-1},\quad \boldsymbol{C}=\kappa\boldsymbol{S}\otimes\boldsymbol{S}, \tag{2}$$

where $\boldsymbol{F}=\nabla_{\boldsymbol{X}}\boldsymbol{x}'$ and $J=\det\boldsymbol{F}$. It is necessary that the characteristic stress tensor $\boldsymbol{S}$ must be *divergence-free* and *symmetric*. Choosing the form of $\boldsymbol{S}=J^{-1}\boldsymbol{F}$ such that $\nabla\cdot\boldsymbol{S}=0$ is always satisfied leads to the pentamode transformation featuring the anisotropic modulus and scalar density [11]. Because the anisotropic stiffness of composites can be readily achieved in a broad frequency range, the pentamode material has served as an appropriate material platform to meet the needs of broadband acoustic control applications [2,7]. Recently, Chen, et al. [2,5] have experimentally designed and verified the pentamode cloaking structure that could conceal objects to be undetectable from underwater sounds. However, it is worth noting that the pentamode transformation is suitable to the case where the transformation deformation gradient $\boldsymbol{F}$ is symmetric or quasi-symmetric in order to ensure the symmetry of $\boldsymbol{S}$ [12]. Thereby, for a general mapping that particularly involves the local coordinate rotation, or rather, the asymmetric transformation, it is usually difficult to select a general form of a divergence-free and symmetric tensor $\boldsymbol{S}$ to implement the pentamode transformation.

Such pursuit of arbitrary control over acoustic propagation is dealt with herein with a focus on the inertial transformation version wherein $\boldsymbol{S}$ in Eq. (1) is set as the identity tensor to avoid the restriction on the form of coordinate mappings. Acoustic parameters in Eq. (2) then become,

$$\boldsymbol{\rho}^{-1}=\rho_0^{-1}\boldsymbol{F}\boldsymbol{F}^T J^{-1},\quad \kappa=\kappa_0 J. \tag{3}$$

* Corresponding author.
E-mail address: zhxming@bit.edu.cn (X. Zhou).

https://doi.org/10.1016/j.eml.2019.100544
2352-4316/

Note that the anisotropic density required here is physically permissible [13,14]. The broadband anisotropic inertia could be realized by fluid–solid composite layers, which have the disadvantage of being potentially impractical due to the presence of fluid phases and the limited density–anisotropy ratio [15]. Therefore, purely solid structures with broadband anisotropic density are desirable for underwater acoustic manipulation. Anisotropic density in solid structures has been attained via the local-resonance effect, but can only be held nearly constant in a narrow frequency region [16,17]. Inspired by the sliding-interface concept in fluid–solid composites for achieving a significant expansion of the working bandwidth, the authors have presented in a previous study a new type of solid metamaterials with fluid-like elasticity and anisotropic density that can be maintained nearly constant in a wide frequency range [18]. Based on this model, functional structures capable of underwater acoustic stretching, shifting, and carpet cloaking were designed, demonstrating clearly the acoustic steering capability of inertial transformation devices [6]. The present work is dedicated to the design of a more general metamaterial model, for which the principal axis of the anisotropic density can be continuously tuned by an arbitrary coordinate mapping to meet the parameter requirement. Further, the design of an underwater acoustic rotator is exemplified to disclose the wave signature of the metamaterials with the mentioned property. Note that the major reason for choosing this example is the fact that the acoustic-rotating device follows from the asymmetric transformation, which is the scenario unsuitable for the pentamode transformation method.

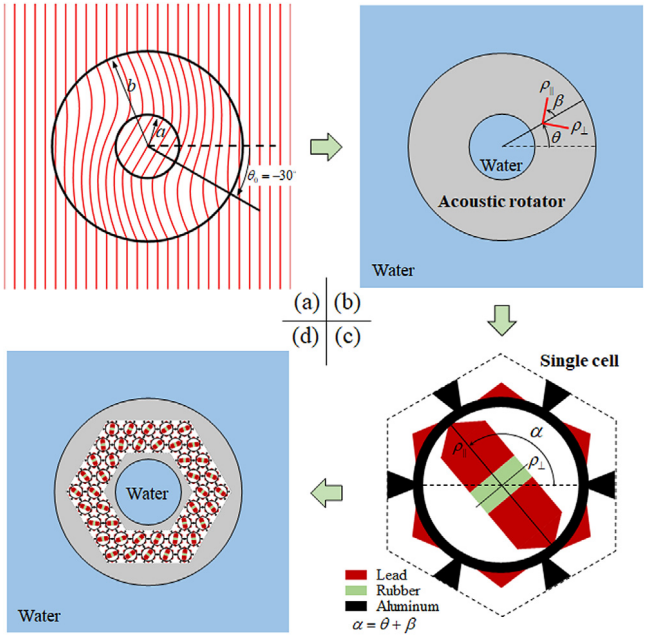

Fig. 1. (a) Coordinate lines of the field-rotating transformation. (b) Configuration of transformation acoustic rotator in which the principal axis of the anisotropic density is marked. (c) Cell structure of the proposed metamaterial with fluid-like elasticity and continuously tuned material axis of the anisotropic density. (d) Schematic profile of the field-rotating device assembled by the metamaterial elements.

2. Models and methods

An acoustic rotator that occupies the cylindrical shell of radius $a < r < b$ has the ability to rotate acoustic fields inside the inner cylinder ($r < a$) by a prescribed angle θ_0 [19], as depicted in Fig. 1(a). In polar coordinates (r, θ), the mapping for this acoustic device aims to keep $r' = r$ in the entire space, and set $\theta' = \theta + \theta_0$ for $r < a$, while let $\theta' = \theta$ for $r > b$. Assuming an arbitrary continuous function $f(r)$, the transformation in the shell region of $a < r < b$ can be expressed as $\theta' = \theta + \theta_0 [f(b) - f(r)] / [f(b) - f(a)]$. The transformation deformation gradient was found to be $\boldsymbol{F} = [(1, 0), (-t, 1)]$ with $t = \theta_0 r f'(r) / [f(b) - f(a)]$. To remove the dependence of t on r, the form function $f(r) = \ln r$ was adopted [20], giving rise to the constant value of $t = \theta_0 / [f(b) - f(a)]$. This arrangement led to the spatially homogeneous anisotropic density, which would facilitate the structure design of the rotator device. According to Eq. (3), the inertial density could be written diagonally in the polar coordinate as $\boldsymbol{\rho} = \mathrm{diag}\left(\rho_\perp, \rho_\parallel\right)$ with $\rho_\perp = 2\rho_0 / \left(t^2 - t\sqrt{t^2+4} + 2\right)$ and $\rho_\parallel = 2\rho_0 / \left(t^2 + t\sqrt{t^2+4} + 2\right)$. The angle between the principal direction and radial axis is given by $\beta = \frac{1}{2} \arccos\left(t / \sqrt{t^2+4}\right)$, as noted in Fig. 1(b). The modulus, namely, $\kappa = \kappa_0$, was unchanged after the mapping because of $\det \boldsymbol{F} = 1$. Moreover, the principal axis of the density was found to continuously change along the angular direction, which likewise implies that the material axis of the corresponding metamaterials should vary continuously. On the contrary, effective stiffness coefficients and principal densities should remain unchanged with the rotation of material axes. Thus, metamaterials possessing these properties would meet all needs of the inertial transformation parameters.

The solid metamaterial developed previously [6] for underwater acoustic manipulation consisted of a solid lattice structure with a low shear resistance for mimicking fluid-like elasticity and was embedded with a sharpened bar inclusion so as to attain the broadband anisotropic density. As opposed to the previous model with hexagonal cell geometry, the aluminum ring-shaped structure [21] designed herein was aimed at hosting the inclusion, as shown in Fig. 1(c). Such improvement led to the possibility of rotating the principal axis of the anisotropic density, which is in line with the bar's axial direction, at an arbitrary angle α. The inclusion structure that shared a similarity with the previous one was adopted, where the soft rubber [21] at the central part plays a critical role of eliminating the influence of the inclusion on the overall stiffness, and the thin connection at the two ends of the central bar is designed for simulating the sliding-boundary effect in fluid–solid composites and is essential to the realization of the broadband anisotropic density. To achieve the fluid-like elasticity for the improved model, the circular ring structures were arranged into a triangular periodic lattice, and adjacent rings were connected by beams with slender ends. The nearest three beams, together with the circular ring in between them, constituted the hexagon-like geometry, which would result in low shear stiffness as verified later. To illustrate, consider the rotation angle $\theta_0 = -30°$, for inner and outer radii of $a = 0.6$ m and $b = 1.8$ m. The required density components could be computed as $\rho_\perp = 0.624\ \rho_0$ and $\rho_\parallel = 1.604\ \rho_0$ with the principal angle of $\beta = -38.3°$. The device was synthesized by allowing the metamaterial cell to repeatedly and periodically occupy the shell region of the rotator (*i.e.*, $a < r < b$), whereas the angular orientation of the inclusion in each cell was arranged following $\alpha = \theta + \beta$. A schematic of the device architecture involving the partial metamaterial elements is illustrated in Fig. 1(d). Notice that the background medium was the water with modulus $\kappa_0 = 2.25$ GPa and mass density $\rho_0 = 10^3$ kg/m^3.

3. Results and discussion

Wave features of the presented metamaterials were investigated through band-structure and effective-medium analyses. First, let us examine the band diagram of the aluminum lattice in Fig. 2(a), in two perpendicular directions (*i.e.*, ΓX and

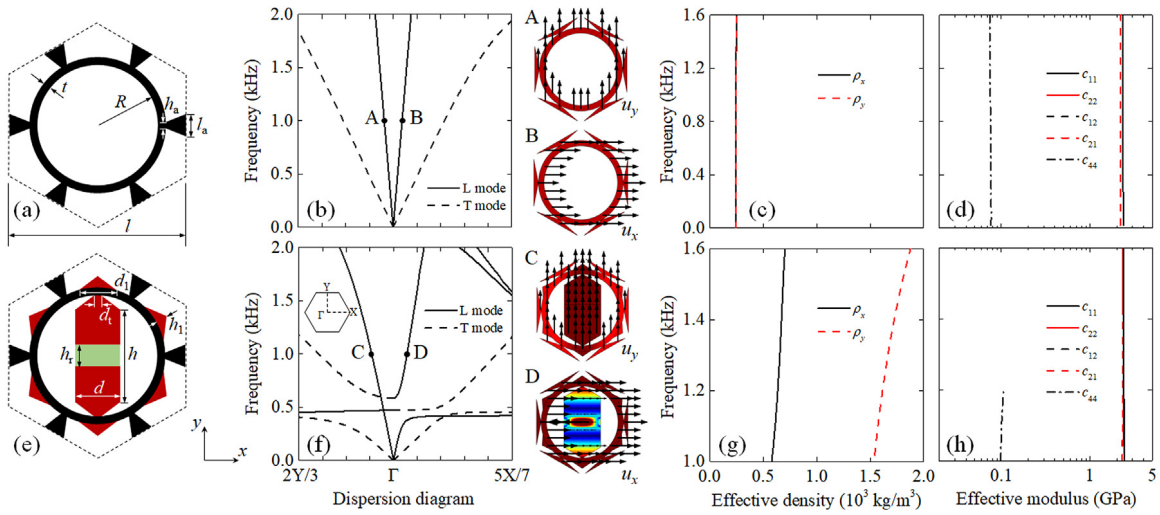

Fig. 2. Geometric structures of the aluminum lattice (a) without and (e) with the attachment, and their respective (b, f) dispersion diagrams and mode shapes at 1 kHz, (c, g) effective inertial densities, and (d, h) effective stiffness parameters. The structural parameters are as follows: R = 23.4 mm, t = 3.6 mm, h_a = 0.5 mm, and l_a = 30 mm for the aluminum lattice; h = 32.8 mm, d = 24 mm, d_t = 0.95 mm, h_r = 7 mm, d_l = 12 mm, and h_l = 3.3 mm for the attachment. The lattice constant of the cell is l = 60 mm.

ΓY), as depicted in Fig. 2(b). Two pairs of weakly dispersive and symmetric branches can be observed, corresponding to the longitudinal (L) and transverse (T) polarizations that are easily recognized from their mode shapes. Next, the effective-medium representation was implemented in the framework of the general anisotropy of both elasticity and inertia. The homogenization medium of the structured metamaterial follows the constitutive equation of $\left[\sigma_{xx}, \sigma_{yy}\right]^T = \left[\left(c_{11}, c_{12}\right), \left(c_{21}, c_{22}\right)\right]\left[\varepsilon_{xx}, \varepsilon_{yy}\right]^T$ and $\sigma_{xy} = 2c_{44}\varepsilon_{xy}$, and the equation of motion of $\left[F_x, F_y\right]^T = \left(-1/\omega^2 S\right)\left[\left(\rho_x, 0\right), \left(0, \rho_y\right)\right]\left[u_x, u_y\right]^T$, where $\sigma_{\alpha\beta}$ and $\varepsilon_{\alpha\beta}$ (α, β = x or y) are the stress and strain fields; F_α and u_α are the net force and displacement, respectively, and S is the cell area. Based on the band-structure results, all effective parameters pertaining to the continuum medium can be retrieved [6,18], as illustrated in Fig. 2(c, d). Specifically in Fig. 2(d), the aluminum lattice exhibited a nearly fluid-like elasticity, where the bulk modulus $c_{11}(\approx c_{22})$ was close to that of water at 2.25 GPa, and the shear stiffness c_{44} was up to one order of magnitude smaller than c_{11}. Fig. 2(c) shows the isotropic inertial density of the lattice, which arises from the uniform displacement response, as verified by the mode shapes of the L branch at 1 kHz in Fig. 2(b).

To acquire the anisotropic density with the desired values, the sharpened bar inclusion was added to each lattice cell, and the lead attachment [21] was deposited at the outer edge of the aluminum ring, increasing the cell weight [Fig. 2(e)]. The band structure of the metamaterial is depicted in Fig. 2(f). Here, the addition of inclusions led to a band gap near 0.5 kHz that interrupts the L branch. Such gap was responsible for the transition from the isotropic density of the pure lattice to the anisotropic one of the metamaterial [6,18]. Moreover, the mode shapes manifested that the inclusion has induced a significant contrast of inertial motion in two perpendicular directions. As a consequence, the anisotropic density can be achieved in the broad frequency range of 1.0–1.6 kHz [Fig. 2(g)], which corresponds to the weakly dispersive regime of the L band above the gap. Notice that the design of the inclusion's geometry follows the guideline that the density component ρ_x is determined by the host lattice, and that ρ_y measures the total weight of the composite [6,18]. Fig. 2(h) illustrates the effective modulus parameters, which are nearly unchanged with the addition of both the inclusion and lead attachment. To sum up, the geometric parameters of metamaterial

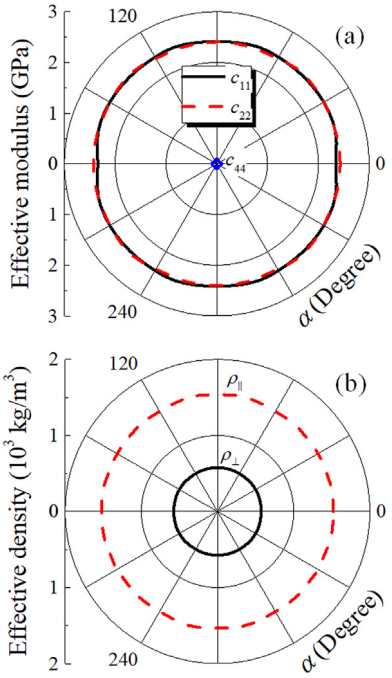

Fig. 3. (a) Effective stiffness and (b) principal values of effective inertial densities for the metamaterial considered in Fig. 2(e) as a function of the rotation angle of the inclusion calculated at a frequency of 1 kHz.

structures can be determined via the decoupling design strategy. More specifically, the overall stiffness is decided by the aluminum lattice only, and the anisotropic density is mostly relevant to the inclusion, which has very little influence on the effective modulus.

While the effective-medium results in Fig. 2 regard the metamaterial model with the orientation angle of $\alpha = 90°$, the effective stiffness and principal densities for an arbitrary α at a specific frequency of 1 kHz are presented in Fig. 3(a) and (b), respectively. The fluid-like elasticity featuring $c_{44} \ll c_{11} \approx c_{22}$ can be observed for all orientation angles of the inclusion. Besides, the circular profile of the density spectrum was observed as well, demonstrating the robustness of anisotropic densities against the

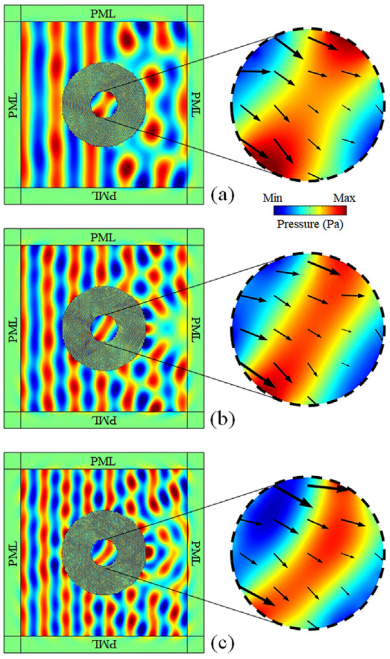

Fig. 4. Simulated pressure field distributions of plane acoustic waves with a frequency of (a) 1 kHz, (b) 1.3 kHz, and (c) 1.6 kHz, incident on acoustic metamaterial rotator immersed in the water background.

rotation of material axes. Note that the principal densities (*i.e.*, $\rho_{\perp}$ and $\rho_{\parallel}$) were retrieved from the dispersion diagrams in the band directions in line with the inclusion's orientation.

The field-rotating functionality of the device can be evaluated through acoustic pressure distributions of the interior and exterior regions of the rotator, exited by a plane wave propagating rightwards with the frequency of 1.0, 1.3, and 1.6 kHz, are shown in Fig. 4(a) to (c), respectively, with which numerical simulations were performed using the software COMSOL Multiphysics. In the internal region enclosed by the rotator, the wave front that still remains nearly flat assumed a clockwise rotation and redirected toward the prescribed angle of $-30°$. Moreover, the field-rotating effect could be observed in three different frequencies, which verifies the broadband acoustic-control capability of the metamaterial. Unwanted external scatterings in the forward direction were a result of a discrepancy of densities between the designed and target values, and of the insufficiently small shear stiffness. In future studies, the wave manipulation performance of these metamaterials may be improved through optimization of the microstructure to minimize the parameter gaps.

4. Conclusions

The wave dispersion and effective-medium analyses demonstrated the ability of the proposed broadband metamaterial to possess the continuously tuned material axes of anisotropic density and fluid-like elasticity, as well as the capability of assembling the transformation device with an acoustic-rotating functionality. In particular, even with the different angular orientation of the material axes, the cell structures can still be easily connected, owing to the cell's regular profile and the decoupling design strategy of the metamaterial [6]. Accordingly, transformation devices with the arbitrary acoustic-control capability could be designed by using the proposed model. The presented metamaterial consists of physically realizable materials; thereby, the experimental realization of arbitrary acoustic manipulation in an underwater environment could be anticipated.

Declaration of competing interest

The authors declare that they have no known competing financial interests or personal relationships that could have appeared to influence the work reported in this paper.

Acknowledgments

This work was supported by the National Natural Science Foundation of China (grant numbers 11872111, 11622215, 11521062, and 11572039) and 111 project (grant number B16003).

References

[1] L. Zigoneanu, B.-I. Popa, S.A. Cummer, Three-dimensional broadband omnidirectional acoustic ground cloak, Nature Mater. 13 (4) (2014) 352–355.
[2] Y. Chen, M. Zheng, X. Liu, Y. Bi, Z. Sun, P. Xiang, J. Yang, G. Hu, Broadband solid cloak for underwater acoustics, Phys. Rev. B 95 (18) (2017) 180104.
[3] B.-I. Popa, L. Zigoneanu, S.A. Cummer, Experimental acoustic ground cloak in air, Phys. Rev. Lett. 106 (25) (2011) 253901.
[4] S. Zhang, C. Xia, N. Fang, Broadband acoustic cloak for ultrasound waves, Phys. Rev. Lett. 106 (2) (2011) 024301.
[5] Y. Chen, X. Liu, G. Hu, Latticed pentamode acoustic cloak, Sci. Rep. 5 (2015) 15745.
[6] J. Dong, Y. Zhao, Y. Cheng, X. Zhou, Underwater acoustic manipulation using solid metamaterials with broadband anisotropic density, J. Appl. Mech. 85 (12) (2018) 121007.
[7] X. Su, A.N. Norris, C.W. Cushing, M.R. Haberman, P.S. Wilson, Broadband focusing of underwater sound using a transparent pentamode lens, J. Acoust. Soc. Am. 141 (6) (2017) 4408–4417.
[8] C.N. Layman, C.J. Naify, T.P. Martin, D.C. Calvo, G.J. Orris, Highly anisotropic elements for acoustic pentamode applications, Phys. Rev. Lett. 111 (2) (2013) 024302.
[9] J.B. Pendry, D. Schurig, D.R. Smith, Controlling electromagnetic fields, Science 312 (2006) 1780.
[10] A.N. Norris, Acoustic cloaking theory, Proc. R. Soc. A 464 (2097) (2008) 2411–2434.
[11] G.W. Milton, A.V. Cherkaev, Which elasticity tensors are realizable?, J. Eng. Mater. Technol. 117 (4) (1995) 483–493.
[12] Y. Chen, X. Liu, G. Hu, Design of arbitrary shaped pentamode acoustic cloak based on quasi-symmetric mapping gradient algorithm, J. Acoust. Soc. Am. 140 (5) (2016) EL405.
[13] G.W. Milton, J.R. Willis, On modifications of Newton's second law and linear continuum elastodynamics, Proc. R. Soc. Lond. Ser. A Math. Phys. Eng. Sci. 463 (2079) (2007) 855–880.
[14] Z. Wang, X. Zhou, Time domain characteristics of wave motion in dispersive and anisotropic continuum acoustic metamaterials, J. Acoust. Soc. Am. 140 (6) (2016) 4276–4287.
[15] B.I. Popa, S.A. Cummer, Homogeneous and compact acoustic ground cloaks, Phys. Rev. B 83 (22) (2011) 224304.
[16] R. Zhu, Y.Y. Chen, Y.S. Wang, G.K. Hu, G.L. Huang, A single-phase elastic hyperbolic metamaterial with anisotropic mass density, J. Acoust. Soc. Am. 139 (6) (2016) 3303–3310.
[17] R. Zhu, X.N. Liu, G.L. Huang, H.H. Huang, C.T. Sun, Microstructural design and experimental validation of elastic metamaterial plates with anisotropic mass density, Phys. Rev. B 86 (14) (2012) 144307.
[18] Y. Cheng, X. Zhou, G. Hu, Broadband dual-anisotropic solid metamaterials, Sci. Rep. 7 (1) (2017) 13197.
[19] X. Jiang, B. Liang, X.Y. Zou, L.L. Yin, J.C. Cheng, Broadband field rotator based on acoustic metamaterials, Appl. Phys. Lett. 104 (8) (2014) 083510.
[20] H.Y. Chen, C.T. Chan, Transformation media that rotate electromagnetic fields, Appl. Phys. Lett. 90 (24) (2007) 241105.
[21] The Young's modulus, Poisson's ratio, and mass density are 71 GPa, 0.33 and 2700 kg/m^3 for aluminum, respectively; 41 GPa, 0.37 and 11600 kg/m^3 for lead; 2 MPa, 0.49 and 1200 kg/m^3 for soft rubber.